Frontiers in Heat and Mass Transfer (FHMT), 18, 17 (2022)
DOI: 10.5098/hmt.18.17

Global Digital Central
ISSN: 2151-8629

Frontiers in Heat and Mass Transfer

Available at www.ThermalFluidsCentral.org

MULTI-OBJECTIVE OPTIMIZATION OF DRYING ENERGY CONSUMPTION AND JET IMPINGEMENT FORCE ON A MOVING CURVED SURFACE

Ali Chitsazan[a], Georg Klepp[a], Mohammad Esmaeil Chitsazan[b], Birgit Glasmacher[c]

[a]*Institute for Energy Research, Ostwestfalen-Lippe University of Applied Sciences and Arts, Lemgo 32657, Germany*
[b] *Research Institute of Education, Ahvaz, Iran*
[c]Institute for Multiphase Processes, Leibniz University Hannover, Hannover 30167, Germany

ABSTRACT

For the optimization of the impinging round jet, the pressure force coefficient and drying energy consumption on the moving curved surface are set as the objective functions to be minimized simultaneously. SHERPA search algorithm is used to search for the optimal point from multiple objective tradeoff study (Pareto Front) method. It is found that the pressure force coefficient on the impingement surface is highly dependent on the jet to surface distance and jet angle, while the drying energy consumption is highly dependent on the jet to jet spacing. Generally, the best design study during the multi-objective optimization is found at the maximum jet to surface distance, jet to jet spacing and surface velocity, and also minimum inlet velocity and jet angle.

Keywords: Multiple jets, Heat transfer, Pressure force, Energy consumption, Optimization

1. INTRODUCTION

Jet impingements enhance the heat transfer rate in many industrial applications such as cooling, heating, and drying due to the large amounts of heat and mass transfer between the surface and the working fluid. Jet impingement flow has many applications in the industry such as the cooling of electronic and turbine components, drying of textile and paper, etc. The designer should optimize the design parameters of industrial drying equipment to achieve minimum capital and running costs. Designs that require high jet velocity and temperature aren't attractive due to the high energy costs (Etemoglu and Can, 2013).

Ito et al. (2007) observed that the Nusselt number for both flat and concave surfaces increased as the Re number increased. Li and Corder (2008) found that the secondary peak on the curved surface is seen for the small jet to plate distance (H/d), and the case with a small distance shows a higher heat transfer rate downstream. Ashok Kumar et al. (2009) observed that the average heat transfer coefficient on the curved surface reduces as H/d increases beyond unity. Heo et al. (2012) observed that the heat transfer rate increases with the pitch of orthogonal jet nozzles on a target curved surface. They found that the optimum inclination angle and the pitch of staggered jet nozzles on a concave surface at Reynolds number of 23,000 are 59.09º and 8.074, respectively. Fenot et al. (2008) found that increasing the curvature causes a small growth of Nu number in the impingement region and the curvature produces confinement of the jet flow that decreases the Nu number distribution. Bu et al. (2015) found that decreasing the surface curvature and increasing the jet impingement angle can improve the Nu number at the stagnation point. They determined an optimal H/d=4.5 to achieve the best heat transfer performance on a concave surface.

Some industrial processes such as paper dryer or rolling of sheet stock or external heat transfer to rotating parts require the target surface to move. The selection of an effective speed depends on several factors such as the jet spacing and a time constant associated with the heat and mass transfer rate to or from the target surface. Chattopadhyay (2006) found that the surface velocity affects strongly the flow field over the target surface and reduces the heat transfer rate. Kadiyala and Chattopadhyay (2017) observed that by increasing the surface velocities the heat transfer reduces initially and reaches a minimum and increases again. Maximum heat transfer is achieved for the stationary surface before the transition, while the maximum heat transfer after the transition is achieved at the velocity ratio equal to 6.

Jet force on the surface is typical for impinging jets towards the surface and it is very important in drying applications for force-sensitive products (i.e. paper, fabrics) or force-sensitive surfaces (i.e. painted, coated). The nozzle exit velocity could be limited if the product is sensitive to deformation under the jet impinging force. Nevertheless, in the investigations reported this aspect is often omitted. Wang et al. (2015) found that the force coefficient from a single round jet impinging on a fixed flat surface is highly dependent on the jet to plate distance and relatively insensitive to Re number.

Kamal et al. (2006) stated that the optimum case which satisfies the largest drying rates beside the uniform pressure distributions along the drying plane is S/d = 3.5, H/d=6, and $\theta = 60^{\circ}$. Xing et al. (2013) found that H/d=3 could provide higher heat transfer performance for a variety of crossflow configurations. Specht (2014) found that for single nozzle arrays and hole channels the maximum heat transfer is at optimum S/d=6. For perforated plates, the maximum heat transfer is for S/d=4 and the minimum specific energy consumption is achieved with S/d=8-10. Attalla (2015) shows that the maximum average Nu is achieved at S/d=2. Zhu et al. (2015) found a relationship between the injection height and nozzle spacing (H≈8S) for uniform heat transfer. Bu et al. (2016) determined an optimal H/d=4-5.75 corresponding to the maximum stagnation Nu on a concave surface. Yang et al. (2017) indicated that optimum values of H/d=10, S/d=30, and $\theta=15^{\circ}$ enhance both local and averaged Nu on the concave surface. Chitsazan et al. (2021a, b, c) conducted a single objective optimization for jet impingement heat transfer, force, and drying energy consumption.

A considerable amount of studies has been dedicated to the optimization of jet impingement heat transfer only at optimum values for H/d, S/d, and θ. The optimization of drying energy consumption and the jet impingement force is very rare in literature. The innovative changes are necessary to make the dryer thermally and hydrodynamically more

Global Digital Central
ISSN: 2151-8629

efficient. The scope of this research is to find the optimum value of key design parameters of paper drying machines such as the jet-to-surface distance, jet-to-jet spacing, jet inlet velocity, jet angle, and surface velocity. The drying energy consumption and jet impingement force on a moving curved surface are set as the objective functions to be minimized simultaneously. Multiple objective tradeoff studies (Pareto Front) and the SHERPA algorithm are used for the optimization study.

2. PHYSICAL MODEL

In the following, the conservation laws of mass, momentum, and energy are expressed for an incompressible fluid with the constant fluid properties in steady state form:

$$\frac{\partial U_i}{\partial X_i} = 0 \tag{1}$$

$$U_j \frac{\partial U_i}{\partial X_j} = \frac{\partial}{\partial X_j}\left(\nu \frac{\partial U_i}{\partial X_j}\right) - \frac{1}{\rho}\frac{\partial P}{\partial X_j} \tag{2}$$

$$U_j \frac{\partial \Theta}{\partial X_j} = \frac{\partial}{\partial X_j}\left(\Gamma_\Theta \frac{\partial \Theta}{\partial X_j}\right) + q_\Theta \tag{3}$$

The Reynolds-Averaged Navier Stokes equations are solved for the transport of mean flow quantities with appropriate RANS turbulence models to describe the influence of the turbulent quantities to provide closure relations. Each solution variable in the instantaneous Navier-Stokes equations should be decomposed into an averaged value and a fluctuating component to obtain the Reynolds-Averaged Navier-Stokes equations. The resulting equations for the mean quantities are essentially identical to the original equations, except that an additional term now appears in the momentum transport equation. This additional term, known as the Reynolds stress tensor, has the following definition:

$$T_t = -\overline{U_i' U_j'} \tag{4}$$

The challenge is thus to model the Reynolds stress tensor to close the time-averaged equations. Eddy viscosity models employ the concept of a turbulent viscosity for modeling of Reynolds stress tensor. The most common model is known as the Boussinesq approximation:

$$T_t = 2\nu_t S_{ij} - \frac{2}{3}\delta_{ij} k \tag{5}$$

Where ν_t is the turbulent viscosity, k is the turbulence kinetic energy, δ_{ij} is the Kronecker delta (=1 if i=j, otherwise =0) and S_{ij} is mean strain rate tensor and given by:

$$Sij = \frac{1}{2}\left(\frac{\partial \overline{U} i}{\partial X j} + \frac{\partial \overline{U} j}{\partial X i}\right) \tag{6}$$

Since the assumption that the Reynolds stress tensor is linearly proportional to the mean strain rate and does not consider the anisotropy of turbulence, some two-equation models extend the linear approximation to include the non-linear constitutive relations. The use of hybrid models as a combination of efficient two-equation models is advisable. The Shear Stress Transport (SST) k-ω model as a combination of the k-ε model in the freestream and the standard k-ω model in the inner parts of the boundary layer is an obvious choice. For further details, refer to the STAR-CCM+ user guide.

Figure 1 shows the geometry of the multiple impinging jets and boundary conditions. All jet inlets were modeled as circular planes in the top wall. The incoming flow is assumed to be with constant fluid properties at T = 298.15 K, entered with a uniform velocity profile. The target surface i.e. a moving curved surface was modeled as a no-slip wall held at a constant temperature of T_w = 333.15 K. On all other solid surfaces, no-slip with adiabatic wall boundary conditions is imposed. Constant pressure outlet boundary condition is applied to all open boundaries. The movement of the curved surface is considered along curvilinear axes. A symmetric boundary condition was also applied in the X-Y plane for the central jet to reduce the computational cost.

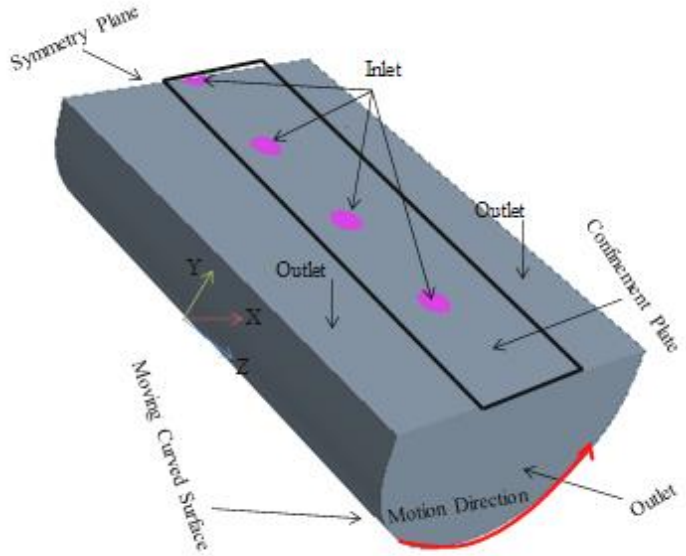

Fig. 1 Schematic of the computational domain

3. DEFINITION OF CHARACTERISTIC NUMBERS

The local heat transfer coefficient is presented in dimensionless form by the Nusselt number:

$$Nu = \frac{hd}{k} = \frac{q}{(T_w - T_j)} . \frac{d}{k_t} \tag{7}$$

Where q is the convective heat flux, T_w is the target wall temperature, T_j is the jet exit temperature, d is the jet exit diameter, k_t is the thermal conductivity of the air at jet exit temperature and h is the local heat transfer coefficient.

Pressure force on the surface is the force that the fluid exerts in the normal direction to the surface. Pressure force on the impingement surface is presented in dimensionless form by a force coefficient C_f as follows:

$$Cf = \frac{P_S A}{0.5\rho V^2 (\pi d^2/4)} \tag{8}$$

Where F is the pressure force on the surface, ρ is the density of the fluid, d is the nozzle diameter, V is the jet exit velocity, P_{st} is the pressure at the stagnation point and A is the surface area.

The specific drying energy consumption is defined as the ratio of the energy for heating the air jet $\dot{H}_j$ to the evaporation enthalpy $\dot{H}_V$:

$$\frac{\dot{H} j}{\dot{H}_V} = \frac{\pi d^2 \rho c_p V}{4S^2}\left(\frac{1}{h} + \frac{T_S - T_a}{\dot{m}_V \Delta h_V}\right) \tag{9}$$

Global Digital Central
ISSN: 2151-8629

In the above equation, T_a is the ambient temperature; c_p is the average specific heat capacity between the jet and the environment temperatures, ρ is the jet density, V is the jet exit velocity from the nozzles with a diameter of d, T_s is the saturation temperature, S is the nozzle to nozzle spacing, $\dot{m}_V$ is the evaporation flux, and Δh_V is the evaporation enthalpy. The air jet temperature is calculated from the condition that the transferred heat has to cover the evaporation enthalpy and the enthalpy to heat the dry material flow from the ambient temperature (T_a) to the saturation temperature (T_s) (Specht, 2014).

4. COMPUTATIONAL DETAILS

The CFD model is set up and run with the commercial code STAR-CCM+ 13.02.013 by CD-Adapco. The final solution was obtained by applying a second-order discretization upwind scheme and the SIMPLE algorithm is used for pressure-velocity coupling. SST k-ω turbulence model is used as recommended by many researchers (Heo et al., 2012; Kadiyala and Chattopadhyay, 2017). The flow in the near-wall regime was simulated using a low-Reynolds number approach. The solution was considered to be converged when the value of the scaled residual of the continuity, momentum, and energy equations is less than 10^{-4}.

An unstructured Polyhedral grid was generated. The local discretization error distribution is calculated by the GCI method (Roache, 2003) shown in Table 1. The overall discretization error for fine and intermediate grids was very small. The intermediate grid is selected as the final grid to reduce the computational cost.

Table 1 Grid parameters of the refinement study at Re =23,000

Grid	Base Size (m)	Cell Number	Max y^+	Average GCI %
Course	0.00192	447,431	0.44	---
Intermediate	0.00127	970,045	0.31	4.12
Fine	0.00088	2,157,431	0.23	2.6

5. OPTIMIZATION METHOD

The designer should optimize the design parameters of industrial drying machines to achieve minimum energy consumption. Jet impingement force on force-sensitive products such as paper is very important in drying applications. Therefore, the pressure force and energy consumption in the dimensionless form are selected as the objective functions to be minimized simultaneously. Optimization for the multiple impinging jets on a moving curved surface has been performed for jet-to-surface distance (H/d), the jet-to-jet spacings (S/d), jet exit velocity (V_j), surface velocity (V_w), and jet angle (θ) as shown in Table 2. Other parameters are held constant as Cr=0.1, d=10mm, T_j= 373.15 K, T_w= 333.15 K and ambient temperature (293.15 K).

Table 2 Design Variables and Design Space

Design variable	Lower bound	Upper bound
H/d	2	10
S/d	2	10
θ	40°	90°
Re number	4337	21685
Relative surface velocity (VR)	0.0034	1
V_j	10 m/s	50 m/s
V_w	0.17 m/s	10 m/s

Multiple objective tradeoff study (Pareto Front) is used for a multi-objective optimization study. This type of optimization study is suited to cases where two objectives are competitive such as lift and drag coefficients. In such cases, there is no single optimum design. Instead, the optimization returns a curve along which all designs are optimum in one objective for a given value in the other objectives, known as the non-dominated design condition. This curve, known as the Pareto front, expresses the optimum trade-off relationship between two competing objectives. Finding the Pareto front for cases where there are more than two competing objectives requires a large number of design evaluations (see Fig. 2). A multiple objective tradeoff study (Pareto front) uses the Multi-Objective SHERPA search algorithm (STAR-CCM+ user guide).

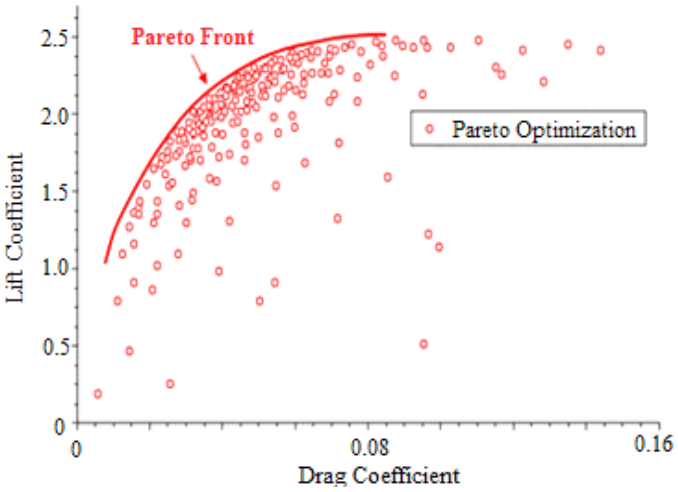

Fig. 2 Multiple objective tradeoff study (Pareto front)

6. RESULTS AND DISCUSSION

6.1 Evaluation of Computational Model

The numerical results of this work have been compared with the literature (Fenot, 2008). The difference between the experiment and the CFD is approximately 15% on average. The agreement between the results is very good and closely followed the same trend (see Fig. 3). The main reason for the sudden decrease of Nu number in the numerical simulation results at the angular distance of 45° could be attributed to the flow separation during flow over a curved surface.

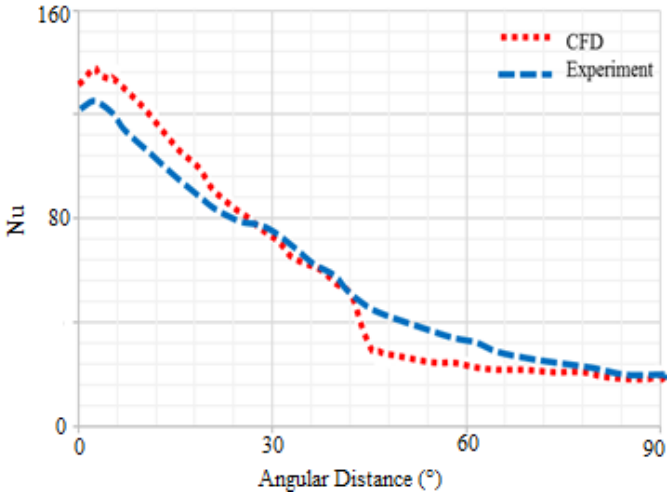

Fig. 3 Comparison of the local Nu along the curvilinear axis on a fixed curved surface between experiments and CFD (H/d=5, S/d=4, Re = 23000, Cr=0.1, VR=0)

6.2 Multi-Objective Optimization

6.2.1 Jet Re number

Figure 4 shows the design study with two logarithmic trend lines during the multi-objective optimization for minimum pressure force coefficient (C_f) and specific drying energy consumption (SDEC) simultaneously for different Reynolds numbers.

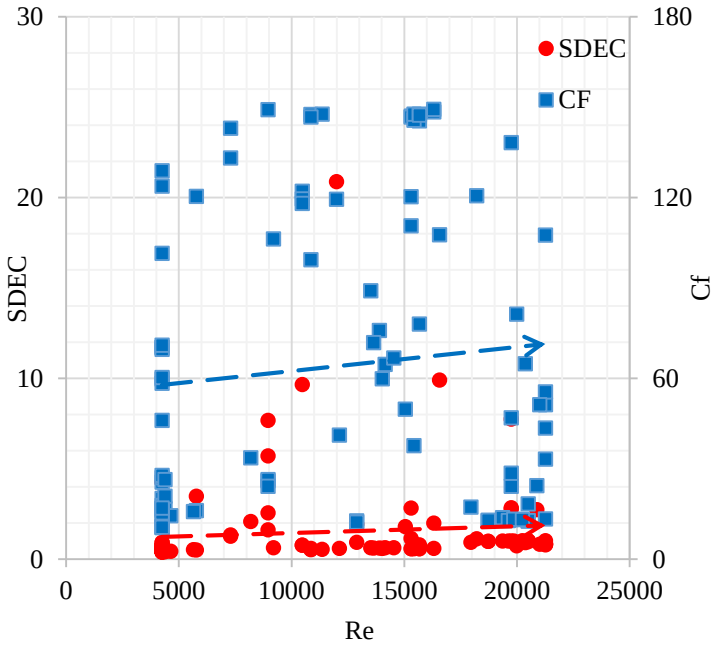

Fig. 4 Design study during the multi-objective optimization for different Re number

The results indicate that the pressure force coefficient increases as the Re number increases and the specific energy consumption is relatively insensitive to the Re number during the multi-objective optimization. These results are in contrast to the results for single-objective optimization for pressure force coefficient (Chitsazan et al., 2021c) where it is relatively insensitive to the jet Reynolds number and also for specific energy consumption (Chitsazan et al., 2021b) where increasing the jet Re number increases the specific energy consumption because the inlet velocity is included in the numerator of the specific energy consumption definition (Eq. 9) and the denominator of the force coefficient definition (Eq. 8). Hereby the best design for multi-objective optimization correlates with low values of jet velocity.

6.2.2 Nozzle to Surface Distance

Figure 5 shows the design study with two logarithmic trend lines during the multi-objective optimization for minimum pressure force coefficient (C_f) and specific drying energy consumption (SDEC) simultaneously for the different nozzle to surface distance (H/d).

Results indicate that the pressure force coefficients on the impingement surface are highly dependent on the vertical nozzle to surface distance. The pressure force coefficients always increase with decreasing H/d, due to the decreasing momentum exchange between the jet flow and the ambient. Hence, the minimum distance is not appropriate for products sensitive to pressure forces. This observation is similar to single-objective optimization (Chitsazan et al., 2021c). The specific energy consumption is relatively insensitive to H/d during the multi-objective optimization in contrast to the result for single-objective optimization (Chitsazan et al., 2021b) where the specific energy consumption increases as H/d increases. Hereby the best design for multi-objective optimization correlates with high values of H/d.

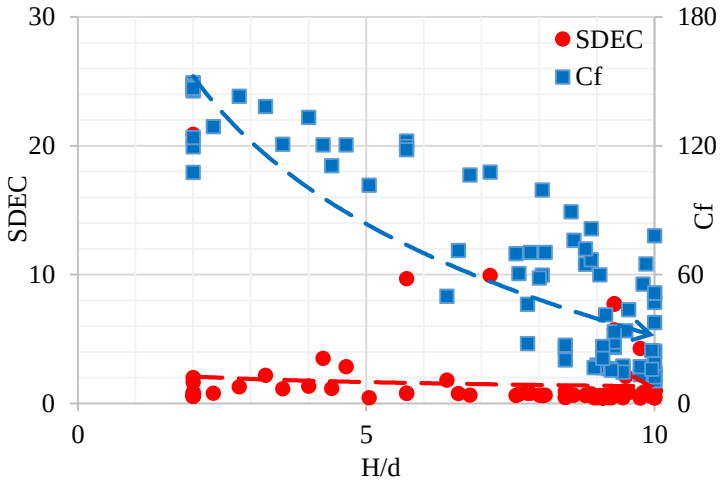

Fig. 5 Design study during the multi-objective optimization for the different nozzle to surface distance

6.2.3 Jet to Jet Spacing

Figure 6 shows the design study with two logarithmic trend lines during the multi-objective optimization for minimum pressure force coefficient (C_f) and specific drying energy consumption (SDEC) simultaneously for the different jet to jet spacing (S/d).

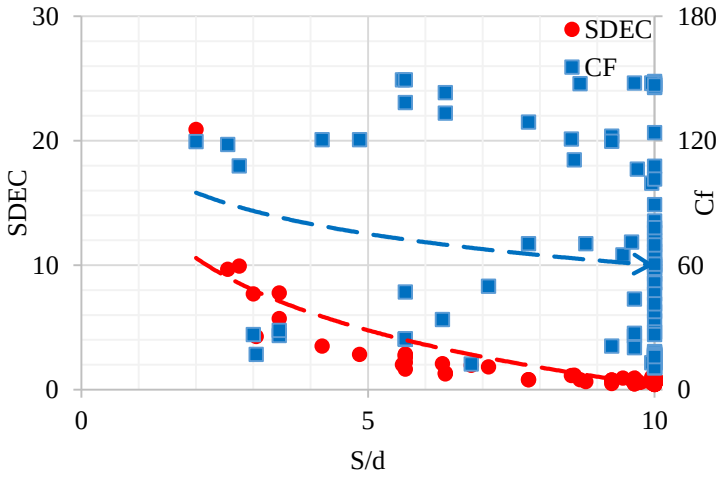

Fig. 6 Design study during the multi-objective optimization for the different jet to jet spacing

The results indicate that the pressure force coefficient decreases with increasing S/d in contrast to the results during the single objective optimization where the pressure force coefficient is relatively insensitive to the S/d (Chitsazan et al., 2021c). The specific energy consumption is highly dependent on the S/d and it always decreases with increasing the S/d due to the role of the S/d in the denominator of energy consumption definition (see Eq. 9). This result is similar to single-objective optimization (Chitsazan et al., 2021b). Hereby the best design for multi-objective optimization correlates with high values of S/d.

6.2.4 Jet Angle

Figure 7 shows the design study with two logarithmic trend lines during the multi-objective optimization for minimum pressure force coefficient (C_f) and specific drying energy consumption (SDEC) simultaneously for different jet angles (θ). The jet angle is varied between 40° and 90° as measured with respect to the horizontal axes.

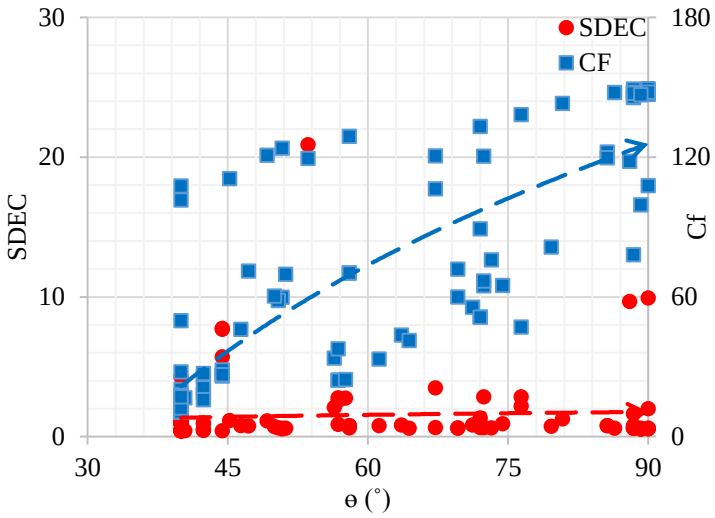

Fig. 7 Design study during the multi-objective optimization for different jet angle

Results indicate that the pressure force coefficient has a strong dependency on the jet angle (ɵ) and increases with increasing the jet angle. This is to be expected because when the jet is directed orthogonal to the surface (90°); it can exert the most pressure upon striking the surface. This result is similar to single-objective optimization (Chitsazan et al., 2021c). Results show that the specific energy consumption is relatively insensitive to the jet angle during the multi-objective optimization. This result is similar to the single objective optimization (Chitsazan et al., 2021b). Hereby the best design for multi-objective optimization correlates with low values of jet angle.

6.2.5 Relative Surface Velocity

Figure 8 shows the design study with two logarithmic trend lines during the multi-objective optimization for minimum pressure force coefficient (Cf) and specific drying energy consumption (SDEC) simultaneously for different velocity ratios (VR).

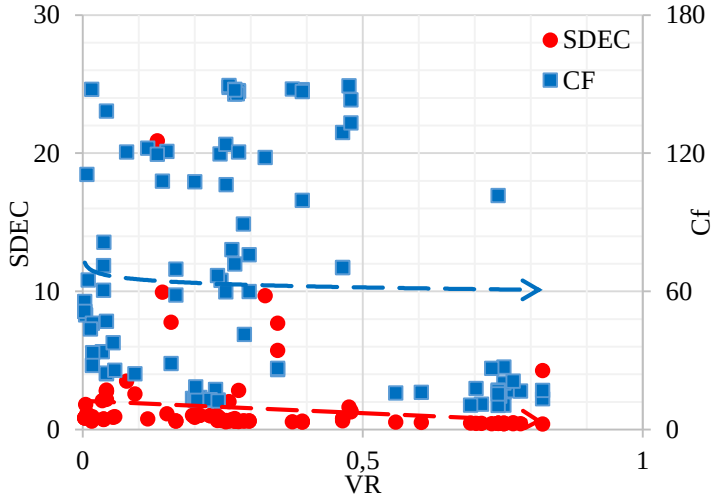

Fig. 8 Design study during the multi-objective optimization for different velocity ratio

Results indicate that the pressure force coefficient is relatively insensitive to the VR during the multi-objective optimization. This result is similar to single-objective optimization (Chitsazan et al., 2021c). Results show that the energy consumption decreases with increasing the VR because of a lower time constant associated with the heat and mass transfer rate to or from the surface. This result is similar to single-objective optimization (Chitsazan et al., 2021b). Hereby the best design for multi-objective optimization correlates with high values of surface velocity.

6.2.6 Comparison between single and multi-objective optimization

In Table 3 a summary of the single objective optimization (Chitsazan 2021a, b, c) and multi-objective optimization results is shown. Optimum jet-to-jet spacing is the same for all objective functions during single and multi-objective optimization and occurs at maximum jet-to-jet spacing within the range examined. A big jet-to-surface distance leads to minimum pressure force coefficients (single and multi-objective optimization), smaller values in contrast lead to maximum average Nu numbers and minimum specific energy consumption. A similar dependence is for the optimum jet angle: minimum value for minimum force coefficient in contrast to maximum value for maximum average Nu and minimum specific energy consumption. The inlet velocity is included in the numerator of the specific energy consumption definition (Eq. 9) and the denominator of the force coefficient definition (Eq. 8). Thus a high inlet velocity leads to a high average Nu number during single objective optimization in contrast to a relative minimum value for the other objective functions. An optimum surface velocity has an almost maximum value for minimum specific energy consumption (single and multi-objective optimization) in contrast to a minimum value for a maximum average Nu number and a minimum pressure force coefficient.

Table 3 Summary of results during the single (Chitsazan, 2021a, b, c) and multi-objective optimization

Objective	H/d	S/d	θ (°)	V_j (m/s)	V_w (m/s)
Max Nu_{ave}	2	10	90	50	0.467879
Min SDEC	3.3	10	88	10	10
Min C_f	10	10	40	15.3731	1.65939
Min C_f and SDEC	9.75	10	40	10	8.2

7. CONCLUSION

The numerical simulations and optimization of multiple circular jets impinging on a moving curved surface are carried out and the commercial CFD package STAR CCM+ is employed with the SST k-ω turbulence model to simulate and optimize a real geometry for industrial drying applications. The designer should optimize the design parameters of industrial drying equipment to achieve minimum capital and running costs. The optimization has been performed for five parameters such as a jet to surface distance, the spacing between the jets, jet inlet velocity, surface velocity, and jet angle. For the optimization of the impinging jet, the pressure force coefficient and specific energy consumption on the concave surface are set as the objective functions to be minimized simultaneously. Hundred design points are selected by the SHERPA Algorithm within the design space. The proper use of the results of this research by a designer should lead to a more reduction in energy consumption and pressure force for industrial drying applications for force-sensitive products or surfaces.

NOMENCLATURE

A_f	open area ratio, total jet area to heat transfer area
A	surface area (m^2)
C_f	force coefficient
d	jet diameter (m)
F	force (N)
H	nozzle-to-target spacing (m)
k_t	thermal conductivity (W/m·K)

Global Digital Central
ISSN: 2151-8629

Nu	Nusselt number
P	pressure (pa)
q	convective heat flux (W/m^2)
R_1	Minor curvature radius (m)
R_2	Major curvature radius (m)
Re	Reynolds number (Re=Vd/ν)
S	jet pitch (m)
S_x	streamwise jet-to-jet distances (m)
S_y	spanwise jet-to-jet distances (m)
T	temperature (K)
V	magnitude of jet exit velocity (m/s)
y+	dimensionless wall distance

Greek letters

k	turbulence kinetic energy (kgm^2/s^2)
ω	specific dissipation rate of turbulence kinetic energy (1/s)
θ	jet inclined angle with respect to the horizontal axes (°)
ρ	density of the fluid (kg/m^3)
ν	kinematic viscosity (m^2/s)

Subscripts

ave: average
j: jet
w: wall

Abbreviation

Cr: curvature ratio; the ratio of minor to the major radius
CFD: computational fluid dynamic
GCI: grid convergence index
VR: velocity ratio; surface to jet velocity
SST: shear stress transport

REFERENCE

Ashok Kumar, M., Prasad, B. V. S. S. S., 2009, "Computational investigations of flow and heat transfer on an effused concave surface with a single row of impinging jets for different exit configurations," *J. Engineering Applications of Computational Fluid Mechanics*, 3, 530-542. https://doi.org/10.1080/19942060.2009.11015289

Attalla M., 2015, "Stagnation region heat transfer for circular jets impinging on a flat plate, experimental heat transfer," *J. Thermal Energy Generation, Transport, Storage, and Conversion*, 28, 139-155. https://doi.org/10.1080/08916152.2013.829134

Bu X., Peng L., Lin G. et al. (2 more authors), 2015, "Experimental study of jet impingement heat transfer on a variable-curvature concave surface in a wing leading edge," *J. Heat and Mass Transfer*, 90, 92-101. https://doi.org/10.1016/j.ijheatmasstransfer.2015.06.028

Bu X., Peng L., Lin G. et al. (2 more authors), 2016, "Jet impingement heat transfer on a concave surface in a wing leading edge: Experimental study and correlation development," *J. Experimental Thermal and Fluid Science*, 78, 199-207. https://doi.org/10.1016/j.expthermflusci.2016.06.006

Chattopadhyay H., 2006, "Effect of surface motion on transport processes due to circular impinging jets – a numerical study," *J. Drying Technology*, 24, 1347-1351. https://doi.org/10.1080/07373930600951117

Chitsazan, A., Klepp, G., Glasmacher, B., 2021a, "Numerical optimization of heat transfer from multiple jets impinging on a moving curved surface for industrial drying machines," *Int. J. Heat and Technology*, 39, 32-40. https://doi.org/10.18280/ijht.390104

Chitsazan, A., Klepp, G., Glasmacher, B., 2021b, "Numerical optimization of drying energy consumption from multiple jets impinging on a moving curved surface," *Int. J. Heat and Technology*, 39, 755-762. https://doi.org/10.18280/ijht.390309

Chitsazan, A., Klepp, G., Chitsazan, M. E., Glasmacher, B., 2021c, "Numerical optimization of pressure force from multiple jets impinging on a moving curved surface for industrial drying machines," *Open J. Fluid Dynamics*, 11, 192-209. https://doi.org/10.4236/ojfd.2021.114012

Etemoglu A.K., Can M., 2013, "Performance studies of energy consumption for single and multiple nozzle systems under impinging air jets," *J. Heat Mass Transfer*, 49, 1057-1070. https://doi.org/10.1007/s00231-013-1137-8

Fenot, M., Dorignac E., Vullierme J.-J., 2008, "An experimental study on hot round jets impinging a concave surface," *J. Heat and Fluid Flow*, 29, 4945–4956. https://doi.org/10.1016/j.ijheatfluidflow.2008.03.015

Heo, M. W., Lee, K. D., Kim, K. Y., 2012, "Parametric study and optimization of staggered inclined impinging jets on a concave surface for heat transfer augmentation," *J. Numerical Heat Transfer, Part A: Applications*, 61, 442-462. https://doi.org/10.1080/10407782.2012.654453

Ito, R., Takeishi, K., Oda, Y., Yoshida, N., 2007, "Heat transfer for round air jets flowing along a concave surface," *In ASME/JSME 2007 Thermal Engineering Heat Transfer Summer Conference collocated with the ASME 2007 InterPACK Conference*, 597-605. https://doi.org/10.1115/HT2007-32616

Kadiyala P.K., Chattopadhyay H., 2017, "Numerical simulation of transport phenomena due to array of round jets impinging on hot moving surface,"*J. Drying Technology*, 35, 1742-1754. https://doi.org/10.1080/07373937.2016.1275672

Kamal R.M., El sayed Mostafa M., Abdel Aziz S.S., 2006, "An experimental study of an oblique multiple circular air jets impingement on a flat plate," *Eight International Congress of Fluid Dynamics and Propulsion*, Egypt.

Li XC, Corder PP., 2008, "Characteristics of cooling of the leading edge with a row of dual impinging jets," *ASME. Heat Transfer Summer Conference*, 2, 625-633. https://doi.org/10.1115/HT2008-56347

Roache P. J., 2003, "Conservatism of the grid convergence index in finite volume computations on steady-state fluid flow and heat transfer," *J. Fluids Engineering*, 125, 731–735. https://doi.org/10.1115/1.1588692

Specht E., 2014, "Impinging jet drying, modern drying technology,"*Volume 5: Process Intensification, First Edition, Published by Wiley-VCH Verlag GmbH & Co. KGaA*.

STAR-CCM+ 13.02.013 user guide by CD-Adapco.

Wang, X. K., Niu, G. P., Yuan, S. Q., Zheng, J. X., & Tan, S. K., 2015, "Experimental investigation on the mean flow field and impact force of a semi-confined round impinging jet," J. *Fluid Dynamics Research*, 47, 025501. https://doi.org/10.1088/0169-5983/47/2/025501

Xing Y., Weigand B., 2013, "Optimum jet-to-plate spacing of inline impingement heat transfer for different crossflow schemes," *J. Heat Transfer*, 135, 072201. https://doi.org/10.1115/1.4023562

Yang B., Chang S., Wu H., Zhao Y., Leng M., 2017, "Experimental and numerical investigation of heat transfer in an array of impingement jets on a concave surface," *J. Applied Thermal Engineering*, 127, 473–483. https://doi.org/10.1016/j.applthermaleng.2017.07.190

Zhu D., Wang Y., Zhu J., 2015, "Heat transfer characteristics of multinozzle air impingement jet during die steel plate cooling progress," *J. Advances in Mechanical Engineering*, 698072. https://doi.org/10.1155/2014/698072